Yuan Gao
Department of Mechanical and Aerospace Engineering,
The Ohio State University,
Columbus, OH 43210
e-mail: gao.1492@osu.edu

Xiguang Huang
Associate Professor
School of Mechanical and Material Engineering,
North China University of Technology,
Beijing, China
e-mail: marchbupt@126.com

Ishan Singh Mann
Department of Mechanical and Aerospace Engineering,
The Ohio State University,
Columbus, OH 43210
e-mail: mann.461@osu.edu

Hai-Jun Su[1]
Fellow ASME
Professor
Department of Mechanical and Aerospace Engineering,
The Ohio State University,
Columbus, OH 43210
e-mail: su.298@osu.edu

A Novel Variable Stiffness Compliant Robotic Gripper Based on Layer Jamming

In this paper, we present a novel compliant robotic gripper with three variable stiffness fingers. While the shape morphing of the fingers is cable-driven, the stiffness variation is enabled by layer jamming. The inherent flexibility makes compliant gripper suitable for tasks such as grasping soft and irregular objects. However, their relatively low load capacity due to intrinsic compliance limits their applications. Variable stiffness robotic grippers have the potential to address this challenge as their stiffness can be tuned on demand of tasks. In our design, the compliant backbone of finger is made of 3D-printed PLA materials sandwiched between thin film materials. The workflow of the robotic gripper follows two basic steps. First, the compliant skeleton is driven by a servo motor via a tension cable and bend to a desired shape. Second, upon application of a negative pressure, the finger is stiffened up because friction between contact surfaces of layers that prevents their relative movement increases. As a result, their load capacity will be increased proportionally. Tests for stiffness of individual finger and load capacity of the robotic gripper are conducted to validate capability of the design. The results showed a 180-fold increase in stiffness of individual finger and a 30-fold increase in gripper's load capacity. [DOI: 10.1115/1.4047156]

Keywords: compliant mechanisms, mechanism design, robot design, soft robots

1 Introduction

Robots are widely considered as the one of the key technologies for numerous fields ranging from manufacturing, medicine, to scientific exploration. Conventional hard robots are typically designed by rigid links with three to six discrete joints aiming for high performance (speed, payload, and accuracy) desired for industrial applications. On the other hand, recently emerging soft/compliant robots are made of highly deformable materials for tasks in unstructured environments that require a larger configuration space. Compared with conventional hard counterpart, robots that are made up of compliant material and structure have many advantages including adaptability, flexibility, durability, and safety to environment [1,2].

Grippers are one kind of robotic manipulators which are meant for grasping and manipulating objects. Although there are many existing grippers with good and stable performance with objects in certain shapes, dealing with irregular objects in an unstructured environment remains challenging [3]. When it comes to grasping irregular and/or fragile objects, rigid grippers may not work as well and even destroy the grasped object. Current rigid grippers based on multi-finger design require many controllable joints to realize high degree-of-freedom, many force sensors to ensure a safe operation and prevent the gripper from crushing the object, and a demanding computational power to decide the magnitude and position of each finger's stress, which introduces a high level of hardware and software complexity. Compliant robotic grippers could be an alternative for gripping tasks thanks to their advantages such as low weight, high adaptability without need for complicated control methods, being inherently safe for human, robustness under impact or collision, and low cost [4]. However, due to the compliance of material and structure, compliant grippers could neither bear much load nor be controlled precisely [5].

To improve the load capacity of compliant grippers, researchers have put forward several variable stiffness methods that are applied in design and control of mechanisms to tune stiffness. A linkage mechanism with tunable rigidity [6] realizes 3.6 times change in stiffness, but this method requires linkage, motors, and other components that increase the structural complexity. Another method that employs low melting point alloy achieves a 25-fold stiffness change [7]. However, melting alloy is time-consuming, and alloys tend to fracture at low strain amounts, which make it unsuitable for the actuator. Magnetorheological elastomer that can be controlled by magnetic field is one of materials adopted to implement tunable stiffness and already used to adjust the spring constant of vibration absorbers [8]. This technique demands extremely flexible elastomer, and it is difficult to pack electromagnets in moving parts, which bring construct problems and make it hard to be applied in actuator.

Material jamming is another technique employed to achieve tunable stiffness. Jamming structures used to vary stiffness in compliant mechanisms consist of a sealed volume filled with materials. In the jamming process, numerous small pieces of material initially in loose state contract under external actuation, which is usually a negative pressure, and transform to a solid-like tight state. Granular and layer jamming that, respectively, use particle and sheet material are two main categories in material jamming. There are researches conducted on granular jamming in the form of robotic joints [9] and manipulators [3,10–13]. Layer jamming shows good performance in many applications. Narang et al. [14] derived an analytical model for two-layer structure and constructed finite element models of multi-layer structure. A jamming structure that consists of only jamming layers and vacuum bag was built and showed a larger stiffness change ratio. However, the structure is passive-driven and cannot restore to the initial position due to the lack of backbone. A manipulator for minimally invasive [15,16] is

[1]Corresponding author.

Contributed by the Mechanisms and Robotics Committee of ASME for publication in the Journal of Mechanisms and Robotics. Manuscript received October 9, 2019; final manuscript received April 26, 2020; published online June 5, 2020. Assoc. Editor: Venkat Krovi.

developed taking advantage of variable stiffness to ensure the safety of patient. A pneumatic variable stiffness gripper based on layer jamming was developed by Lin et al. [17], and it achieved 4.6 times increase in output force for single finger. Zhu et al. [18] developed a fully multi-material 3D printed gripper combining pneumatic actuator and layer jamming technique, which realized robust grasping at acceleration up to 8 m/s^2. Wall et al. [19] integrated both granular and layer jamming to PneuFlex actuators and achieved a maximum eight-fold stiffness increase in layer jamming prototype. A stiffening sheath is designed by Langer et al. [20], and it improved stiffness of continuum robot by a factor up to 24. Latest researches on layer jamming include designing new backbone structure to which layers could be attached [21,22] and medical application [23,24]. In addition, fiber material could also be exploited for jamming application [25]. Compared with other alternatives, layer jamming can make more effective use of pressure, demand less volume to work and realize higher stiffness change ratio, which make layer jamming a good choice for the actuator.

In this study, a variable stiffness compliant actuator is designed by integrating layer jamming technique into a compliant cable-driven skeleton that can achieve one-way bending motion. Layer jamming technique is utilized by attaching four interlocked configured sheets of film at each side face of the backbone and sealing it into a latex airtight bag. A compliant robotic gripper is built by adopting three triangularly distributed actuators as its fingers. Initially, to ensure a rapid and adaptive gripping and safety of human, the gripper is in flexible mode, and three fingers are bent to conform the shape of the grasped object. At the second stage of grasp, the negative pressure is applied to the airtight bag, and sheet films are pressed. The pressure between layers produces a force of static friction that impede the relative movement of layers and hold the gripper in current position, which bring increase in both stiffness and load capacity.

This paper starts with design work of the gripper at Sec. 2. Fabrication details are illustrated in Sec. 3. In Sec. 4, the experiments and measurements for both single finger and gripper are conducted to assess the performance. Also in this section, the analysis of test result is carried out to validate the availability of design and a force control model for a single finger is proposed. Finally, conclusion and future work are presented in Sec. 5.

2 The Design of Compliant Robotic Gripper

The CAD model of the compliant robotic gripper is shown in Fig. 1. The gripper is composed of three fingers that are assembled into a 3D printed palm. Each finger consists of two main parts: compliant skeleton and layer jamming module. The design and function of each part are detailed in following subsections.

2.1 Design of Compliant Backbone. The skeleton of the variable stiffness finger is composed of a long compliant backbone, two cables, a servo motor, an airtight holder, and several fixtures. Figure 2 shows shape and main dimensions of the backbone. The consecutive thin beam in the middle of backbone is 0.8 mm in thickness, which is designed to guarantee the flexibility of backbone. Along the center beam, ten branches are evenly distributed on each side in longitudinal direction. The jamming layers are placed on outer surface of these branches. In the jammed state, the fore of static friction between layers generates a moment to counter the moment introduced by external force, which increases the bending stiffness of the backbone. The semi-elliptical side surface of each branch is meant for supporting the soft latex bag and reducing size of trap caused by sinking of membrane under vacuum.

This backbone is the key to increase the stiffness ratio since it significantly increases the distance between jamming layers on both sides that leverages the resistance moment resulted from friction forces in jamming layers. This allows us employing only several

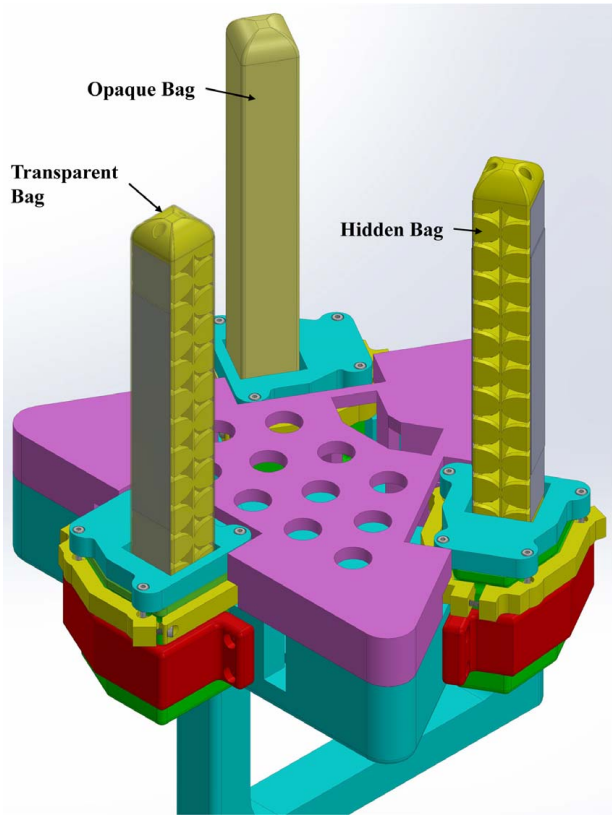

Fig. 1 Isometric view of the compliant gripper CAD model with one latex bag being transparent and another bag being hidden for demonstration

(four–six) sheets to obtain as high as 180 folds increase in stiffness and 30 + folds increase for load carrying capacity. Compared with variable stiffness gripper exploiting pneumatic actuator [17–19], inflatable pneumatic actuator usually has one inextensible substrate as bending center and one extensible top surface. If layers are attached to the substrate [17,18], small distance between layers and bending center will result in a small stiffness change ratio. If layers are attached to the top surface, extended length of the surface will reduce overlap between layers and then decrease stiffness change ratio. In addition, positive pressure source is no longer necessary for tendon driven backbone. Compared with tubular shaped manipulator using layer jamming [16,20], flat surface of

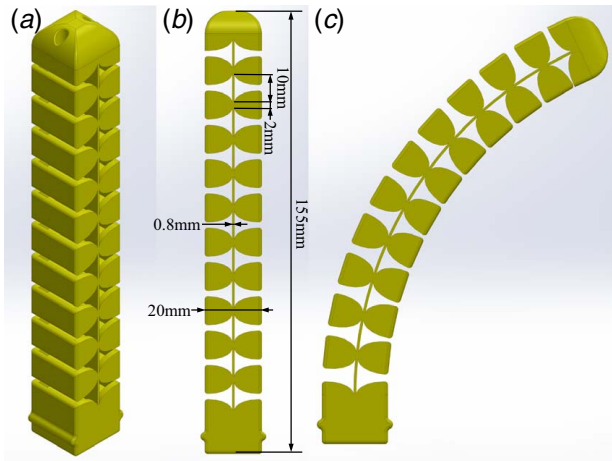

Fig. 2 Views of the backbone: (*a*) isometric, (*b*) front, and (*c*) morphed shape

backbone and interlocked layer configuration enables higher stiffness change ratio in our design.

2.2 Morphing Actuation Method. There are various actuation methods for compliant actuators, and two widely adopted means are variable length tendons (in the form of tension cables or shape memory alloy) and pneumatic actuation. The basic operating principle behind shape memory alloy (SMA) technology is that nickel titanium (NiTi) wire contracts under joule heating that is typically produced by passing electrical currents through the wire, which is non-instantaneous and thus inapplicable for a gripper. Pneumatic actuation that is used to inflate chambers in soft mechanism for achieving desired deformation requires several tubes and valves to work, and it could not be employed due to size constraints. In this work, the method with tension cables driven by servo motors is adopted given its advantages of high accessibility, low volume requirement, and fast response in control.

Tension cables actuation method for the skeleton is implemented by a servo motor and two cables. As is shown in Fig. 3, two driven cables run through the skeleton in longitudinal direction via the small holes in branches with one end fixed to the top of backbone and the other end fixed to servo horn. The bottom ends of two cables are set in the opposite position of the horn and they are straight initially. Based on the design, two cables, respectively, work on either forth or back stroke, which accelerate the back stroke of the actuator and help the finger recover after manipulation.

2.3 Variable Stiffness Via Layer Jamming. With respect to layer jamming technique, interlocked and partially overlapping layers are two widely used configurations for sheets of material. Interlocked setup is employed in our gripper in view of the its higher stiffness ratio [19], and the layout of jamming layers is demonstrated in Fig. 4(*a*). Four interlocked films including two uppers and two lowers are attached to each side of the backbone by gluing one end to either top or bottom of backbone. To implement layer jamming effect, a bag made of soft latex membrane, an airtight vessel, and several fasteners are employed to create hermetic seal. The schematics are shown in Figs. 4(*b*) and 4(*c*).

Depending on whether the layer jamming effect is activated, the actuator has two modes: flexible and locked mode. In the flexible mode, there is no negative pressure supplied to the actuator and backbone can bend and recover easily under actuation of the servo motor with small resistance. The layers on both side of the backbone can conform to the shape of morphed backbone and remain contacted to the surface of branches. In the first phase of

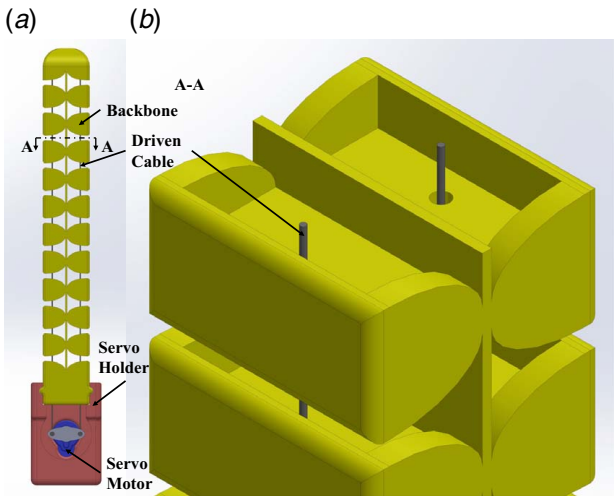

Fig. 3 (*a*) Overview of the actuator skeleton and (*b*) isometric view on cross section A-A

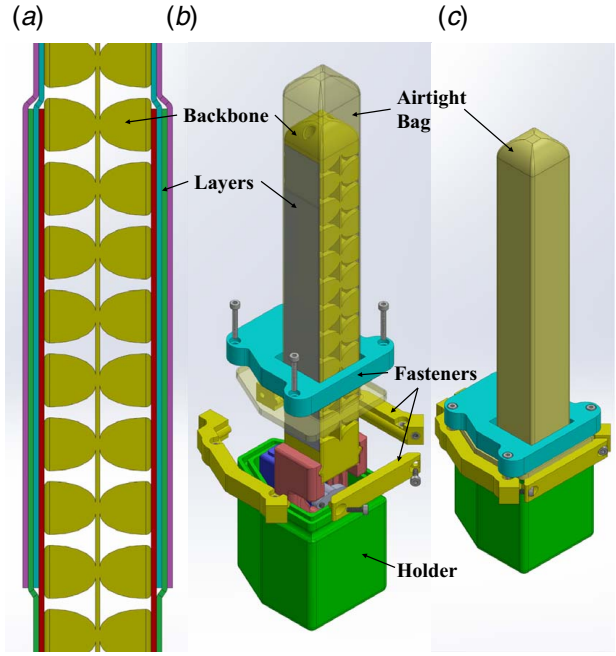

Fig. 4 (*a*) Interlocked layer configuration, (*b*) isometric exploded view of assembled finger with transparent bag, and (*c*) isometric view of assembled finger

gripper working period, fingers are in flexible mode and driven to bend, and a grasp for the object formed by at least three contact points is established. Then, a certain negative pressure is applied inside the bag through a pipe and fingers are transformed to the locked mode. In the locked mode, the pressure on layer-layer, backbone-layer, and bag-layer surfaces increases and hardens the actuator. When object is pulled apart from the gripper by an external force, the static frictional force on layer-layer, backbone-layer, and bag-layer surfaces can generate an antagonistic moment to offset the moment from external force so as to hold the morphed shape of gripper and keep a stable grasp of the object.

Compared with locking tendon by a higher torque servo, implementing layer jamming is more robust since force applied to finger is transmitted to bottom of backbone through layers instead of tendons. Also, a higher torque servo that performs as well and is in similar size cost much higher than combination of smaller torque servo and layer jamming module. In addition, layer jamming saves power/energy during the picking up and transportation stage as long as there is no leakage in the system because vacuum inside finger can lock finger shape. Last but not the least, locking the tendon would allow the finger to change shape while layer jamming can lock the shape.

3 Fabrication Process

The compliant robotic gripper prototype and is shown in Fig. 5. The fabrication including assembly the process is described.

The backbones of compliant actuator and fasteners of finger are made of polylactic acid (PLA) filament and 3D printed with 0.2 mm in layer thickness and 40% in infill density in a MakerBot Z18 printer. However, for the holder, 100% infill density and a higher printing temperature are necessary for airtightness. The skeleton of actuator is driven by a Hitec HS-65HB+ servo motor installed in servo holder. Fishing line, which is 0.7 mm in average diameter, is adopted as driven cable. The two ends of the fishing line are fixed to either skeleton or servo arm using electric soldering iron.

Jamming layers are made of Dura-Lar film with thickness of 0.127 mm and cut into rectangles that are 18 mm in width and

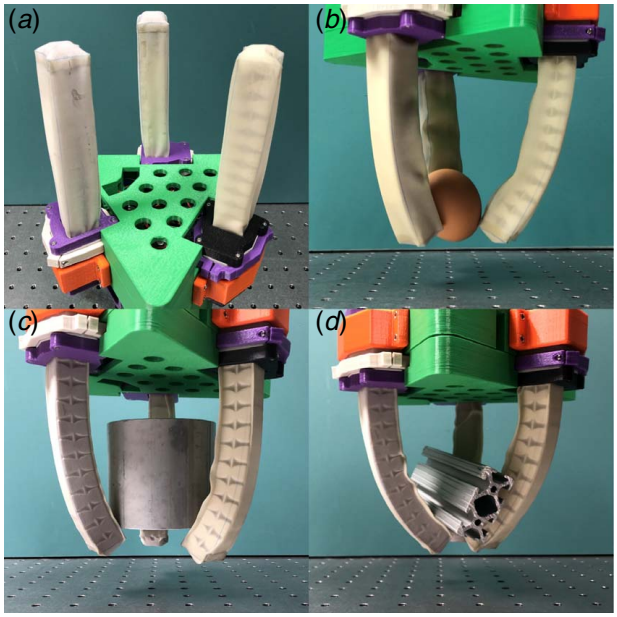

Fig. 5 (*a*) The prototype of the compliant gripper. Panels (*b*), (c), and (*d*) are the grasps of egg, aluminum column, and profile, respectively.

110 mm in length using a laser cutter. Four layers are glued to each side of the actuator in an interlocked configuration. The vacuum bag is fabricated by cropping and gluing the latex membrane with thickness of 0.203 mm into a cuboid shape with one open surface. Then, fix the skeleton in airtight holder by friction between contact surface and wrap the backbone and top of holder using latex bag. The fasteners work for establishing hermetically sealed seam between bag and holder. Note that this method allows motor to move freely inside the vacuum bag without the need of considering the sealing of servo connection part and provides convenience for future maintenance. An air tube is glued to the surface of the holder at one end and connects to a vacuum pump at the other end. All three fingers are secured to a 3D printed gripper palm. A vacuum pump is fixed at the palm of gripper to generate the negative pressure. The interaction between the gripper prototype and some fragile and irregular-shaped objects is shown in Figs. 5(*b*)–5(*d*).

4 Force Control and Displacement Control Models

In order to control the finger, here, we derive the basic model of a single backbone without layers based on the pseudo-rigid-body model (PBRM) method. More specifically, we aim to derive two kinds of analytical open loop control model: force control and displacement control. The former requires the derivation of the relationship of the actuation force F with the bending angle θ of the deflected finger beam. And the latter seeks the relationship of the actuation displacement ΔL with the bending angle θ. We detailed the derivation in the following sections.

4.1 The Pseudo-Rigid-Body Model. The finger backbone can be modeled as a sequence of n compliant segments (length l and thickness a) separated by relatively rigid spacers (thickness t) as shown in Fig. 6(*a*). Let L be the undeflected length of the flexible beam and d be the distance between two driven cables, respectively. When the actuation cable is pulled by the servo motor, a force F is applied to the last spacer in the direction perpendicular to the spacer and the compliant backbone is bent to angle θ.

The pseudo-rigid-body (PRB) model of this backbone is shown in Fig. 6(*b*), in which the compliant flexural segments are simplified as torsion springs at the middle points of the flexural segments.

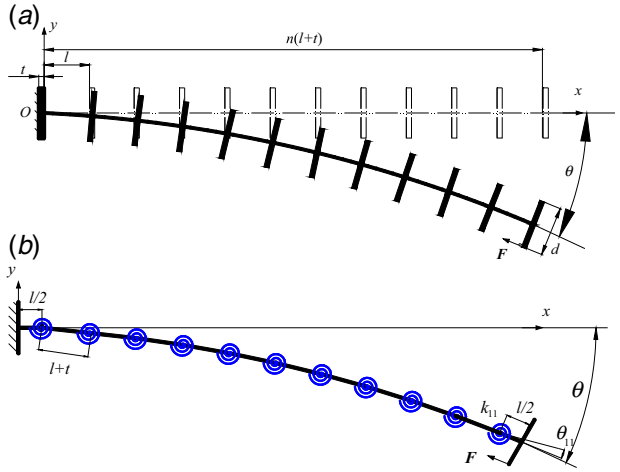

Fig. 6 (*a*) The schematic view of a single finger and (*b*) its pseudo-rigid-body model. *F* represents the actuator force in cable.

4.2 Calculate the Bending Angle. To determine the actuation force and stiffness of the compliant finger, let us study the PRB model of a single segment shown in Fig. 7(*a*). The spring constant in the PRB model is

$$k_i = \frac{EI}{l} = \frac{Ea^3 b}{12l}, \quad i = 1, \ldots, n \tag{1}$$

where E is Young's modulus of beam material and the cross section of the flexural beam is assumed to be a a (in-plane thickness) by b (out-of-plane thickness) rectangle.

Since the bending angle of each segment is relatively small and the tension force in the cable is constant along its length. Therefore, we assume each torsion spring is subject to same bending moment $M = Fd/2$, which produces a bending angle

$$\theta_i = \frac{M}{k_i} = \frac{6Fdl}{Ea^3 b}, \quad i = 1, \ldots, n \tag{2}$$

As a result, the total bending angle is calculated as

$$\theta = \sum_{i=1}^{n} \theta_i = \frac{6nFdl}{Ea^3 b}, \quad i = 1, \ldots, n \tag{3}$$

This gives us a linear relationship of the bending angle θ with the cable force F.

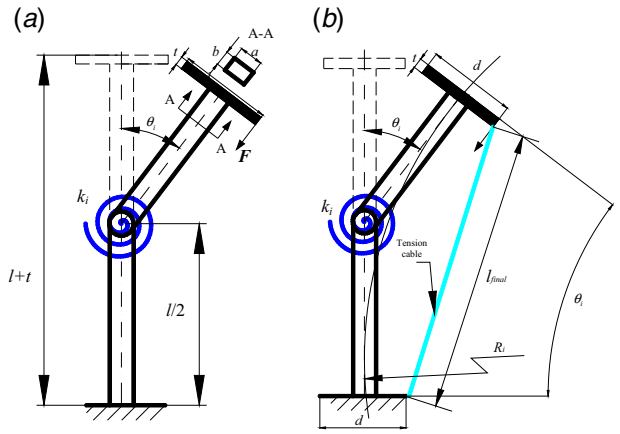

Fig. 7 (*a*) The schematic view of one segment and (*b*) its pseudo-rigid-body model; *F* represents the actuator force in cable

Because the in-plane thickness of the rigid spacer (20 mm) is much larger than that of compliant segment, the deformation of rigid spacers is trivial and not taken into consideration.

4.3 Calculate the Variation of Cable Length. If we apply kinematic control to the compliant finger, we have to derive the relationship of the extension of the actuation cable ΔL with respect to the corresponding bending angle θ. For convenience, let us define the radius of curvature of each compliant segment by

$$R_i = \frac{l}{\theta_i} = \frac{nl}{\theta}, \quad i = 1, \ldots, n \tag{4}$$

And by Fig. 7(*b*), we can determine the cable length for one segment after the bending as

$$l_{final} = 2\left(R_i - \frac{d}{2}\right)\sin\left(\frac{\theta_i}{2}\right), \quad i = 1, \ldots, n \tag{5}$$

The shortening of the actuation cable for one segment is calculated as

$$\Delta L_i = l - l_{final}, \quad i = 1, \ldots, n \tag{6}$$

And the total variation of the actuation cable is

$$\Delta L = \sum_{i=1}^{n} \Delta L_i = n(l - l_{final}), \quad i = 1, \ldots, n \tag{7}$$

To obtain the relationship of ΔL and the total bending angle θ, substituting Eqs. (4) and (5) into Eq. (7) yields

$$\Delta L = n\left[l - 2\left(\frac{nl}{\theta} - \frac{d}{2}\right)\sin\left(\frac{\theta}{2n}\right)\right] \tag{8}$$

4.4 Calculate the Variation of Cable Length in Terms of Actuation Force. Now to relate ΔL to the actuation force F, we can substitute Eq. (3) into Eq. (8) to obtain

$$\Delta L = n\left[l - \left(\frac{Ea^3b}{3Fd} - d\right)\sin\left(\frac{3Fdl}{Ea^3b}\right)\right] \tag{9}$$

The values of all geometric parameters in our prototype are given in Table 1. However, since our fingers are 3D printed in polylactic acid (PLA) material, the Young's modulus of the prototype is unknown and needs to be measured. To do so, we designed and carried out experiment to measure the relationship of the variation of cable length ΔL and the actuation force F.

First, we clamp the root of finger using a vise along the vertical direction. Second, the actuation cable is tied to the test head of Mark-10 force sensor in horizontal direction. The force sensor is mounted on a horizontal travel track with a displacement sensor recording the movement of force sensor. Third, we manually drive the travel track which pulls the actuation cable and the pulling force of actuation cable bends the finger. Fourth, we record the readings from the force sensor and the displacement sensor. The experimental data is shown as the discrete dots in Fig. 8.

Table 1 Numerical values for parameters used in the PRB model

Parameters	Symbol	Value	Unit
Number of segments	n	11	–
In-plane thickness of flexures	a	0.8	mm
Out-of-plane thickness of flexures	b	20	mm
Thickness of spacers	t	2	mm
Length of flexures	l	10	mm
Distance from cable to center beam	d	12	mm
Fit Young's Modulus	E	2.66	GPa

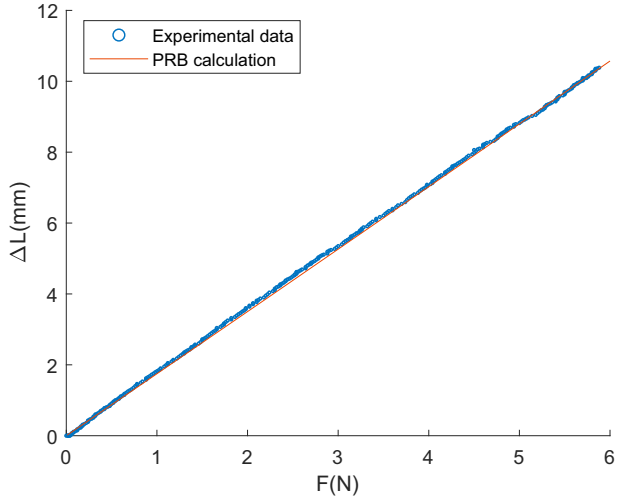

Fig. 8 The variation of cable length ΔL versus actuation force F. The straight line is the theoretical model with the fit young's modulus $E = 2.66$ GPa and the dots are experimental data.

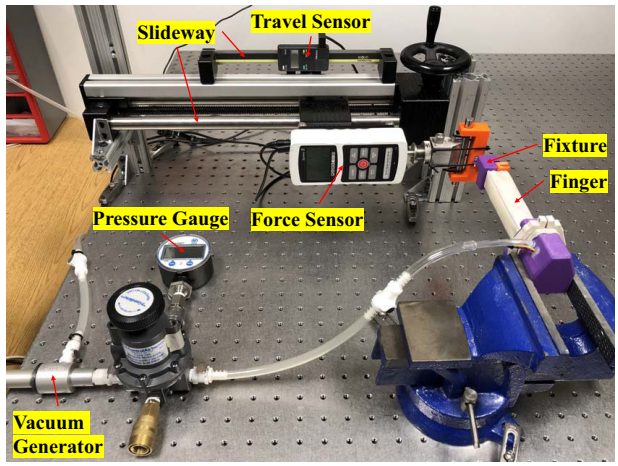

Fig. 9 Setup of single finger stiffness test

To find the Young's modulus of 3D printed PLA material, we employed Eq. (9) to fit the experimental data. It turns out that the best fit returns a value of $E = 2.66$ Gpa, which is a reasonable value according to properties of 3D printed PLA materials. And the theoretical result derived from Eq. (9) is plotted as the continuous line shown in Fig. 8.

5 Experimental Tests and Analysis of Results

In this section, experiments are conducted respectively on a single finger and the whole gripper to test the performance and validate the hypothesis that layer jamming can significantly increase the stiffness of compliant mechanism.

5.1 Single Finger Stiffness Test

5.1.1 Test Setup. Figure 9 shows the setup of the finger stiffness test. One finger is secured horizontally to eliminate the influence from gravity. A MARK-10 force sensor and a travel sensor are installed on a horizontal slideway with a crank handle in the end that is used to drive two sensors along the slideway. Fixture

at top of the finger consists of three 3D printed components, a shaft fixed to end of force sensor, a pair of shafts and bearing allowing frictionless longitudinal displacement, and a ball joint which can rotate freely. Such configuration ensures that the force applied to finger is exactly in tracking direction of force sensor and eliminate error from other trivial forces. A pipe connected to the finger is employed to vacuum the bag. During the test, a set of different pressures are applied to the finger to induce the layer jamming effect. Then the crank handle is turned manually to drive the sensor and push the finger. To obtain static data, force is recorded every 0.5 mm after a 10 s sample time over the total 10 mm travel. Five repeated tests are conducted for each pressure and data is averaged for precision. The gradient of force-displacement curve is defined as the stiffness of finger.

5.1.2 Analysis of Testing Result. In the test, six sets of data under pressures from the list {0, 2.5, 5, 7.5, 10, 12.5} psi are collected and plotted as separate points in Fig. 10. Higher the pressure is, larger the force is under same displacement. For each non-zero pressure case, the force–displacement curve has three sections: pre-slip section, transition section, and full-slip section as reported in Ref. [14]. Within pre-slip section, every group has a linear relation between force and displacement because the force of friction between jammed layers, which play most important role in jamming effect, is lower than maximum force of static friction. When the friction force reaches the maximum static friction force, the curve transforms to transition region in which layers start to slip and the gradient of curve, the stiffness of finger, start to drop until all contact area of layers become slipped and the curve turn into full-slip section. In full-slip section, the slope of the curve maintains at a constant value while displacement keep increasing. The force at start point of transition section has a positive correlation with given pressure, which agree with the assumption that higher negative pressure increase maximum static frictional force between layers. The initial stiffness of the finger achieved a 180-fold increase from 0.008 N/mm under zero pressure to the average 1.522 N/mm enhanced by layer jamming, which validates the availability and high efficiency of layer jamming enabled variable stiffness method.

5.1.3 A Control Model for Finger Stiffness. A well-known model for fitting the transition region from static to kinetic friction is Dahl model [26] governed by equation:

$$f(x) = \beta(1 - e^{-\alpha x}) \tag{10}$$

where x is the relative displacement of two contact surfaces and $f(x)$ is the frictional force between surfaces. Also, $\alpha > 0$ and $\beta > 0$.

According to the experimental data demonstrated in Fig. 10, the force–deflection curve has three phases. The first two could be fit to the exponential function based on the Dahl model and the last one is a linear function. Based on this hypothesis, a control model for force–deflection relation of single finger under different pressures is developed as

$$F(x) = \begin{cases} a(p)(1 - e^{-b(p)x}) & 0 \le x \le x_1(\mathrm{p}) \\ c(p)x + d(p) & x > x_1(\mathrm{p}) \end{cases} \tag{11}$$

where $x_1(p)$ is the turning point from phase 2 (transition) to phase 3 (slip) and $a(p)$, $b(p)$, $c(p)$, $d(p)$ are coefficients of the piece-wise function. Parameters $a(p)$, $b(p)$, $x_1(p)$ are obtained by fitting experimental data with cubic polynomials, which are written as

$$x_1(p) = 0.000134p^3 - 0.0426p^2 + 0.9402p + 1.4490 \tag{12a}$$

$$a(p) = -0.000879p^3 - 0.0165p^2 + 0.9048p + 0.2448 \tag{12b}$$

$$b(p) = -0.000651p^3 + 0.0209p^2 - 0.2282p + 1.0681 \tag{12c}$$

And parameters $c(p)$, $d(p)$ for the slipping phase 3 can be obtained by applying the first- and second-order continuity constraints at the transition point x_1 for the piece-wise function, which are written as

$$c(p) = a(p)b(p)e^{-b(p)x_1(p)} \tag{12d}$$

$$d(p) = a(p)(1 - e^{-b(p)x_1(p)}) - a(p)b(p)x_1(p)e^{-b(p)x_1(p)} \tag{12e}$$

The curves generated from the control model under different non-zero pressures are shown as the solid black line in Fig. 10.

5.2 Load Capacity Test of the Entire Gripper

5.2.1 Test Setup. The setup of gripper load capacity test is demonstrated in Fig. 11. The gripper is vertically installed to the aluminum frame. A MARK-10 force sensor and a travel sensor are assembled on a vertical slideway for measuring the force–displacement relationship. A lightweight ball of 80 mm diameter is used as the object of grasping and fixed to the end of force sensor by steel rod. To generate precise negative pressure inside the bag, rather than the integrated pump, vacuum pipe is chosen to induce

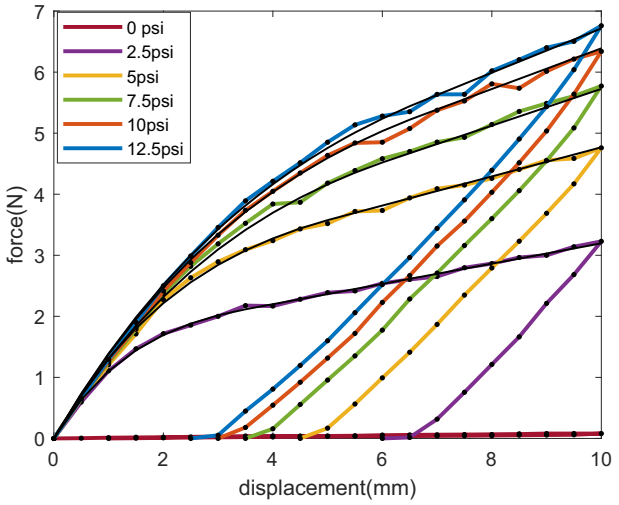

Fig. 10 Experimental data (discrete dots) from finger stiffness tests and fit control model (thin curves)

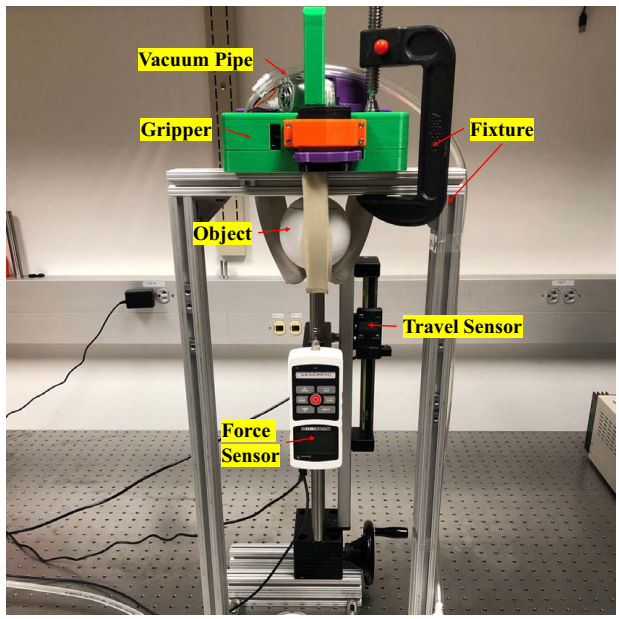

Fig. 11 Setup of gripper load capacity test

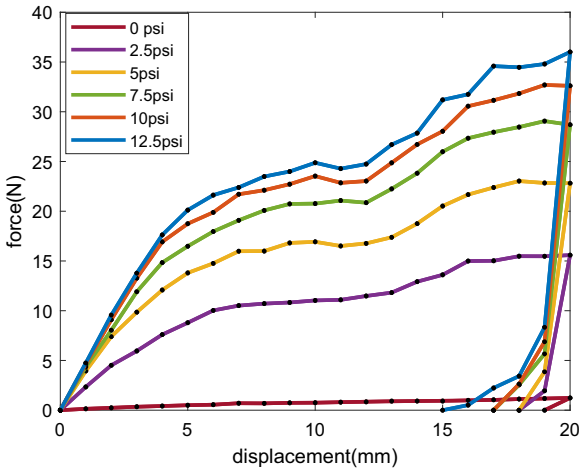

Fig. 12 Experimental data from the load capacity test. All curves have three phases: (1) pre-slipping (the nearly linear portion in the beginning), (2) transition (partially slipping in the middle), and (3) slipping (the nearly flat portion at the end).

the layer jamming effect. During the test, the compliant backbone is actuated at first to morph the finger and fit itself to object. Then, a certain negative pressure generated by vacuum pipe actuate the layer jamming effect and harden each finger. By turning the crank handle of the slideway, two sensors can move downward slowly and a tension force in the rod will drag the object out of gripper. Force data are recorded every 1 mm after 10 s sample time over total 20 mm displacement, and three repeated experiments are carried out for each pressure. Force and displacement relation is measured under six different pressures including {0, 2.5, 5, 7.5, 10, 12.5} psi to test the load capacity and stiffness increase.

5.2.2 Analysis of Testing Results. The experimental data of load capacity test are shown in Fig. 12. According to the curve, the behavior of the gripper under non-zero pressure consist of three phases: pre-slip, transition, and full-slip phases, which meets the characteristic of single finger. Within the pre-slip phase where displacement is small, the curve is in a linear pattern. Once the force reaches the initial force of transition region, the overall stiffness of gripper decreases, and the gradient of curve go down gradually. However, in full-slip phase, the gripping force first converge to a certain value, then the slope of curve increases and decreases again, and the force stay in a higher value finally. The gripping force consists of two parts: normal force on contact surfaces of each finger and frictional force. At the start of movement, the normal force is predominant and friction is static, which leads the curve follow same mode as of single finger. As displacement increases, the normal force reaches upper limit while frictional force keeps increasing to maintain the grasp. At around 12 mm, the angle of finger reaches angle of friction, which means the object start slip relative to finger and the contact point move downward. For new touch point, the threshold of normal force increases and thus force can grow with displacement until it gets to a higher limit.

Table 2 Initial stiffness and load capacity of the gripper

Pressure (psi)	Primary stiffness (N/mm)	Load capacity (N)
0	0.14	1.18
2.5	2.34	15.51
5	3.94	22.90
7.5	4.33	28.74
10	4.61	32.38
12.5	4.75	35.09

Two important criteria to judge performance of the gripper are initial or primary stiffness and load capacity. Higher primary stiffness promises a more stable and firmer grasp under external force or impact. With respect to this gripper, the counteractive force has two or more thresholds, and here, we choose force around 20 mm as load capacity of the gripper. For each pressure, the stiffness of pre-slipping phase and average force in slip phase are listed in Table 2.

From Fig. 12 and Table 2, the non-slipping stiffness of non-zero pressure group is increasing with pressure. The enhanced initial stiffness conforms to result from single finger test, and it indicates that rigidity of the gripper could be significantly increased via the layer jamming technique. In addition, the load capacity has a positive relationship with given pressure, which also agrees with single finger testing results. We observed a 34-fold increase for the initial stiffness of the gripper from 0.14 N/mm ($p = 0$) to maximum 4.75 N/mm ($p = 12.5$ psi). And load capacity increased from 1.18 N ($p = 0$) to 35.09 N ($p = 12.5$ psi). The load capacity of gripper depends on the pressure that enables jamming effect and higher the pressure is, more load the gripper can bear.

The stiffness ratio is given by dividing pressurized stiffness by non-pressure stiffness. For zero pressure case of gripper, unlike single finger experiment in which the force is applied perpendicular to the vacuum bag, the object is pulled downwards and frictional force between the object and vacuum bag will significantly increase the stiffness of the gripper because the antagonistic force in backbone is relatively small. The increase in stiffness of unjammed gripper result in a smaller increase ratio of gripper's stiffness.

6 Conclusions and Future Work

In this paper, a novel compliant robotic gripper with variable stiffness is developed by integrating layer jamming technique to cable-driven actuator. We detailed the design and fabrication process of the gripper. An analytical model based on the pseudo-rigid-body method was developed for predicting deflection of a single finger under actuation force. We have conducted a series of experimental tests of individual fingers and the entire gripper. The initial stiffness of single finger achieves a 180-fold increase and is proved to be hold before external force raise to a critical value that has positive correlation with given pressure. An exponential control model for the stiffness of single finger is constructed on the basis of test data. The overall stiffness and load capacity of the gripper are measured, and a 34-fold and 30-fold increase is observed, respectively, with the layer jamming effect.

Future work includes developing an analytical model of finger's stiffness based on friction of layers for a comprehensive understanding and optimizing the structure. Also a more sophisticated model for calculating the actuation force for both with and without layer jamming in order to more accurately control the gripper and achieve better performance.

References

[1] Rus, D., and Tolley, M. T., 2015, "Design, Fabrication and Control of Soft Robots," Nature, **521**(7553), pp. 467–475.
[2] Trivedi, D., Rahn, C. D., Kier, W. M., and Walker, I. D., 2008, "Soft Robotics: Biological Inspiration, State of the Art, and Future Research," Appl. Bionics Biomech., **5**(3), pp. 99–117.
[3] Brown, E., Rodenberg, N., Amend, J., Mozeika, A., Steltz, E., Zakin, M. R., Lipson, H., and Jaeger, H. M., 2010, "Universal Robotic Gripper Based on the Jamming of Granular Material," Proc. Natl. Acad. Sci. U. S. A., **107**(44), pp. 18809–18814.
[4] Wood, R., and Walsh, C., 2013, "Smaller, Softer, Safer, Smarter Robots," Sci. Transl. Med., **5**(210), p. 210ed19.
[5] Manti, M., Cacucciolo, V., and Cianchetti, M., 2016, "Stiffening in Soft Robotics: A Review of the State of the Art," IEEE Rob. Autom. Mag., **23**(3), pp. 93–106.
[6] She, Y., Su, H.-J., Lai, C., and Meng, D., 2016, "Design and Prototype of a Tunable Stiffness Arm for Safe Human-Robot Interaction," ASME 2016 International Design Engineering Technical Conferences and Computers and Information in Engineering Conference, Charlotte, NC, Aug. 21–24, American Society of Mechanical Engineers, p. V05BT07A063.

[7] Schubert, B. E., and Floreano, D., 2013, "Variable Stiffness Material Based on Rigid Low-Melting-Point-Alloy Microstructures Embedded in Soft Poly(Dimethylsiloxane) (PDMS)," RSC Adv., **3**(46), pp. 24671–24679.
[8] Deng, H.-x., Gong, X.-l., and Wang, L.-h., 2006, "Development of An Adaptive Tuned Vibration Absorber With Magnetorheological Elastomer," Smart Mater. Struct., **15**(5), pp. N111–N116.
[9] Hauser, S., Robertson, M., Ijspeert, A., and Paik, J., 2017, "JammJoint: A Variable Stiffness Device Based on Granular Jamming for Wearable Joint Support," IEEE Rob. Autom. Lett., **2**(2), pp. 849–855.
[10] Cheng, N. G., Lobovsky, M. B., Keating, S. J., Setapen, A. M., Gero, K. I., Hosoi, A. E., and Iagnemma, K. D., 2012, "Design and Analysis of a Robust, Low-Cost, Highly Articulated Manipulator Enabled by Jamming of Granular Media," 2012 IEEE International Conference on Robotics and Automation, Saint Paul, MN, May 14–18, pp. 4328–4333.
[11] Al Abeach, L., Nefti-Meziani, S., Theodoridis, T., and Davis, S., 2018, "A Variable Stiffness Soft Gripper Using Granular Jamming and Biologically Inspired Pneumatic Muscles," J. Bionic Eng., **15**(2), pp. 236–246.
[12] Amend, J., Cheng, N., Fakhouri, S., and Culley, B., 2016, "Soft Robotics Commercialization: Jamming Grippers From Research to Product," Soft Rob., **3**(4), pp. 213–222.
[13] Li, Y., Chen, Y., Yang, Y., and Wei, Y., 2017, "Passive Particle Jamming and its Stiffening of Soft Robotic Grippers," IEEE Trans. Rob., **33**(2), pp. 446–455.
[14] Narang, Y. S., Vlassak, J. J., and Howe, R. D., 2018, "Mechanically Versatile Soft Machines Through Laminar Jamming," Adv. Funct. Mater., **28**(17), p. 1707136.
[15] Kim, Y., Cheng, S., Kim, S., and Iagnemma, K., 2012, "Design of a Tubular Snake-Like Manipulator With Stiffening Capability by Layer Jamming," 2012 IEEE/RSJ International Conference on Intelligent Robots and Systems, Vilamoura, Portugal, Oct. 7–12, pp. 4251–4256.
[16] Kim, Y., Cheng, S., Kim, S., and Iagnemma, K., 2013, "A Novel Layer Jamming Mechanism With Tunable Stiffness Capability for Minimally Invasive Surgery," IEEE Trans. Rob., **29**(4), pp. 1031–1042.
[17] Lin, K.-Y., and Gupta, S. K., 2017, "Soft Fingers With Controllable Compliance to Enable Realization of Low Cost Grippers," *Biomimetic and Biohybrid Systems*, Mangan, M., Cutkosky, M., Mura, A., Verschure, P. F., Prescott, T., Lepora, N., eds., Lecture Notes in Computer Science, Springer International Publishing, pp. 544–550.
[18] Zhu, M., Mori, Y., Wakayama, T., Wada, A., and Kawamura, S., 2019, "A Fully Multi-Material Three-Dimensional Printed Soft Gripper With Variable Stiffness for Robust Grasping," Soft Rob., **6**(4), pp. 507–519.
[19] Wall, V., Deimel, R., and Brock, O., 2015, "Selective Stiffening of Soft Actuators Based on Jamming," 2015 IEEE International Conference on Robotics and Automation (ICRA), Seattle, WA, May 26–30, pp. 252–257.
[20] Langer, M., Amanov, E., and Burgner-Kahrs, J., 2018, "Stiffening Sheaths for Continuum Robots," Soft Rob., **5**(3), pp. 291–303.
[21] Santiago, J. L. C., Godage, I. S., Gonthina, P., and Walker, I. D., 2016, "Soft Robots and Kangaroo Tails: Modulating Compliance in Continuum Structures Through Mechanical Layer Jamming," Soft Rob., **3**(2), pp. 54–63.
[22] Deshpande, A. R., Tse, Z. T. H., and Ren, H., 2017, "Origami-Pnspired Bi-Directional Soft Pneumatic Actuator With Integrated Variable Stiffness Mechanism," 2017 18th International Conference on Advanced Robotics (ICAR), Hong Kong, China, July 10–12, pp. 417–421.
[23] Hadi Sadati, S. M., Noh, Y., Elnaz Naghibi, S., Kaspar, A., and Nanayakkara, T., 2015, "Stiffness Control of Soft Robotic Manipulator for Minimally Invasive Surgery (MIS) Using Scale Jamming," *Intelligent Robotics and Applications*, Liu H., Kubota, N., Zhu, X., Dillmann, R., Zhou, D., eds., Lecture Notes in Computer Science, Springer International Publishing, pp. 141–151.
[24] Tognarelli, S., Brancadoro, M., Dolosor, V., and Menciassi, A., 2018, "Soft Tool for Gallbladder Retraction in Minimally Invasive Surgery Based on Layer Jamming," 7th IEEE International Conference on Biomedical Robotics and Biomechatronics (Biorob), Enschede, Netherlands, Aug. 26–29, pp. 67–72.
[25] Brancadoro, M., Manti, M., Grani, F., Tognarelli, S., Menciassi, A., and Cianchetti, M., 2019, "Toward a Variable Stiffness Surgical Manipulator Based on Fiber Jamming Transition," Front. Rob. AI, **6**(12).
[26] Dahl, P. R., 1968, "A Solid Friction Model," AEROSPACE CORP EL SEGUNDO CA, May, Technical Report, TOR-0158(3107-18)-1.